SCIENTIFIC REP🞂RTS

Roles of Oxygen and Hydrogen in Crystal Orientation Transition of Copper Foils for High-Quality Graphene Growth

Junxiong Hu[1,2,*], Jianbao Xu[1,3,*], Yanfei Zhao[4], Lin Shi[5], Qi Li[1], Fengkui Liu[1], Zaka Ullah[1], Weiwei Li[1,6], Yufen Guo[1,6] & Liwei Liu[1]

The high-quality graphene film can be grown on single-crystal Cu substrate by seamlessly stitching the aligned graphene domains. The roles of O_2 and H_2 have been intensively studied in the graphene growth kinetics, including lowering the nucleation sites and tailoring the domain structures. However, how the O_2 and H_2 influence Cu orientations during recrystallization prior to growing graphene, still remains unclear. Here we report that the oxidation of Cu surface tends to stabilize the Cu(001) orientation while impedes the evolution of Cu(111) single domain during annealing process. The crystal orientation-controlled synthesis of aligned graphene seeds is further realized on the long-range ordered Cu(111) substrate. With decreasing the thickness of oxide layer on Cu surface by introducing H_2, the Cu(001) orientation changes into Cu(111) orientation. Meanwhile, the average domain size of Cu foils is increased from 50 μm to larger than 1000 μm. The density functional theory calculations reveal that the oxygen increases the energy barrier for Cu(111) surface and makes O/Cu(001) more stable than O/Cu(111) structure. Our work can be helpful for revealing the roles of O_2 and H_2 in controlling the formation of Cu single-crystal substrate as well as in growing high-quality graphene films.

Chemical vapor deposition (CVD) method on Cu substrates has emerged as a promising technique for realizing high-quality[1] and large-scale[2] graphene films, which can be scaled up to meter in size by employing roll-to-roll (R2R) method[3]. However, CVD-grown graphene films are usually polycrystalline and consist of numerous grains separated by grain boundaries[4,5], which remarkably degrade their electrical and mechanical properties[6,7]. In order to suppress the grain boundaries, an efficient approach is found to align the graphene domain orientation on a single-crystalline catalyst surface, and then seamlessly coalesce adjacent aligned islands to form uniform monocrystalline graphene. Various efforts have been made to achieve the well-ordered substrates, including the use of expensive single-crystal Ge(110)[8], Ni(111)[9] and Cu(111)[10]. On the contrary, thermal recrystallization in commercial polycrystalline Cu is a versatile way to produce long-range ordered substrate. For instance, the aligned graphene can be grown on the large Cu(111) grain annealed by several hours[11]. By further polishing the surface, the seamless stitching was realized by merging the neighbor graphene domains[12]. Recently, the aligned square domains were also grown on single-crystal Cu(001) surface[13]. In these studies, a precise control of long-range crystalline in Cu substrates is critical for obtaining the well-aligned graphene domains.

For the roles of O_2 and H_2 in the graphene growth kinetics, previous study reported that the O_2 can lower nucleation density[14–16] and reduce the energy barrier for carbon precursor attachment to the edges of graphene[14,17], thus the growth rate of single-crystal graphene can be increased[18]. Besides, the role of H_2 has been

[1]Key Lab of Nanodevices and Applications, Suzhou Institute of Nano-Tech and Nano-Bionics, Chinese Academy of Sciences (CAS), Suzhou, 215123, P. R. China. [2]Department of Physics, Institute of Low-dimensional Carbons and Device Physics, Shanghai University, Shanghai, 200444, P. R. China. [3]College of Materials Sciences and Opto-Electronic Technology, University of Chinese Academy of Sciences, Beijing, 100049, P. R. China. [4]Nano-X, Suzhou Institute of Nano-Tech and Nano-Bionics, Chinese Academy of Sciences (CAS), Suzhou, 215123, P. R. China. [5]Platform for Characterization &Test, Suzhou Institute of Nano-Tech and Nano-Bionics, Chinese Academy of Sciences (CAS), Suzhou, 215123, P. R. China. [6]Suzhou Graphene Nanotechnology Co., Ltd., Suzhou, 215123, P. R. China. *These authors contributed equally to this work. Correspondence and requests for materials should be addressed to L.L. (email: lwliu2007@sinano.ac.cn)

reported to act as an etching reagent that tailors the domain structure[19,20] and terminates the graphene edges to form few layers[21,22]. Therefore, the study of the roles of O_2 and H_2 in the crystal orientation transition of underlying substrate is a prerequisite for achieving precise control of substrate for single-crystalline graphene growth[23,24].

In this work, we designed 3 schemes to control the degree of oxidation by introducing H_2 at different heat treatment stages, obtaining 3 different thicknesses of oxidation layers measured by X-ray photoelectron spectroscopy (XPS), to study how the Cu oxides affects the substrate orientation as well as grain size. In order to reveal the role of O_2 in crystal orientation transition of Cu foils, the density functional theory (DFT) calculations were conducted to study the effect of O_2 on the stabilities of Cu(001) and Cu(111). After obtaining the Cu(111) single domain, the well-aligned hexagonal graphene domains showing similar orientations were grown by ambient pressure CVD(APCVD). Understanding the roles of O_2 and H_2 in the crystal orientation transition of Cu foil is beneficial for the growth of well-aligned graphene arrays on single domain Cu foils. This work using the roll to roll or batch to batch process can deliver scalable production of high-quality graphene films.

Results

Characterizations of the evolution of single domain Cu(111).
During thermal treatments of Cu foils in the tube furnace, the main source of oxygen mostly can be divided into three parts: (a) the trapped air in quartz tube; (b) the native oxide layer on Cu surface; (c) the impure gas source and tiny leakages from environment. According to the sources of oxygen, we designed 3 schemes to control the degree of oxidation through introducing H_2 at different heat treatment stages. The corresponding orientations and grain sizes of Cu foils annealed under 3 schemes are shown in Fig. 1. Before heating, the purging process was conducted to minimize the trapped air in CVD chamber (see method). In scheme 1, in order to introduce relatively high level of oxygen, only the Ar gas without H_2 was introduced during heating and annealing, and in this scheme the Cu foil was subjected to the above mentioned three sources of oxygen. Figure 1a shows a layer of mosaic patterns formed on Cu surface. Electron backscatter diffraction (EBSD) map shows that the Cu surface owns many randomly oriented grains with size 50–100 μm (Fig. 1d), while the X-ray diffraction (XRD) reveals that the Cu has only Cu(001) orientation (Fig. 1g). The difference between EBSD and XRD results can be attributed to the different penetration depths. XRD can probe the depth of micrometers while EBSD just reveals the information from tens of nanometers thickness of Cu surface[25]. When the quartz-tube was not purged, the grain size of Cu foil was further reduced to 5–10 μm (Supplementary Fig. S1). In scheme 2, in order to introduce the medium level of oxygen, we introduced H_2 during heating. However, annealing was still performed under Ar flow. In this scheme, the trapped air and native oxide layer on Cu surface can be removed and the oxygen sources only came from impure gas and tiny leakages. Figure 1b shows that the mosaic patterns on Cu surface start to disappear. EBSD map (Fig. 1e) shows that most of the orientations in Fig. 1d have been transformed to Cu(111) plane. The Cu(111) orientation is further confirmed by XRD profile (Fig. 1h), as a main peak at ~42° is assigned to Cu(111) diffraction. Meanwhile, the grain size increases from 50 μm (scheme 1) to 1000 μm (scheme 2).

In scheme 3, in order to completely suppress the oxidation, the H_2 was introduced in the processes of both heating and annealing. EBSD image shows that the Cu surface has become single domain Cu(111) and been free from grain boundaries, in the meantime, grain size increases to larger than 1000 μm (Fig. 1f) (Supplementary Fig. S2). The XRD analysis also reveals the single Cu(111) oriented grain (Fig. 1i). Furthermore, the Cu(111) orientation can be obtained in 1 min (Supplementary Fig. S3e,f). However, without introduction of H_2 flow (under Ar atmosphere), even though the annealing time was extended to 180 min, the Cu foil still remained in Cu(001) orientation. Nevertheless, followed by introducing H_2 for 1 min, surprisingly, the Cu(111) orientation can be obtained again (Supplementary Fig. S3a–d). The combined analysis of EBSD and XRD clearly proves that the introduction of H_2 tends to assist the evolution of Cu(111) orientation.

In order to reliably achieve single domain Cu(111), other thermodynamics parameters such as temperature, pressure and cooling rate were also investigated (Supplementary Fig. S4). The high temperature up to 1040 °C, near to melting point of Cu foil (1088 °C), was necessary to obtain Cu(111) orientation[11,23,24]. However, when the quartz-tube pressure was decreased to 150 Pa, the Cu(111) orientation can be achieved at 1010 °C, indicating that the decreasing pressure can reduce the orientation-transition temperature for Cu(111)[26,27]. In addition, when the cooling rate was maintained at 0.3 °C/s, the XRD profiles show that apart from Cu(111), other phases such as Cu(001) and Cu(220) will also precipitate upon cooling. Once the cooling rate exceeds 0.9 °C/s, the impure phases can be suppressed efficiently, indicating that fast cooling was in favor of Cu(111) evolution[28].

Characterizations of the aligned graphene domains and continuous film grown on single domain Cu(111).
Based on the obtained single domain Cu(111) substrates, the graphene was further grown on the ordered Cu(111) substrate by ambient pressure CVD (APCVD)[29,30], as shown in Fig. 2. In order to investigate the graphene growth at early stage, we intentionally limited the growth time to produce the individual grains (Fig. 2a). In this partial coverage graphene, the well-aligned hexagonal graphene arrays display the similar orientations, which are indicated by the white dashed arrows. The whole sample exhibits the same feature (Supplementary Fig. S5). When the two identical orientations of islands are merged together, which are indicated by the white arrows, the grain boundaries between adjacent islands may be completely suppressed by the commensurate stitching[12], providing a reliable and efficient strategy for the synthesis of wafer-scale single-crystal graphene.

The uniformity of continuous graphene film was further evaluated by optical microscopy. Figure 2b shows an optical micrograph of full coverage of graphene film. The uniform color contrast of the optical image indicates that the graphene film has an excellent thickness uniformity[31]. The inset in Fig. 2b shows a typical Raman spectrum with peaks for monolayer graphene, including a 2D-band with a full width at half-maximum (FWHM) of ~36 cm^{-1} located at ~2680 cm^{-1}. In addition, the I_{2D}/I_G ratio is ~2.7. Both FWHM and I_{2D}/I_G ratio are on the merits for monolayer graphene[32]. Moreover, the defect density n_{do} can be calculated from the empirical formula[33]:
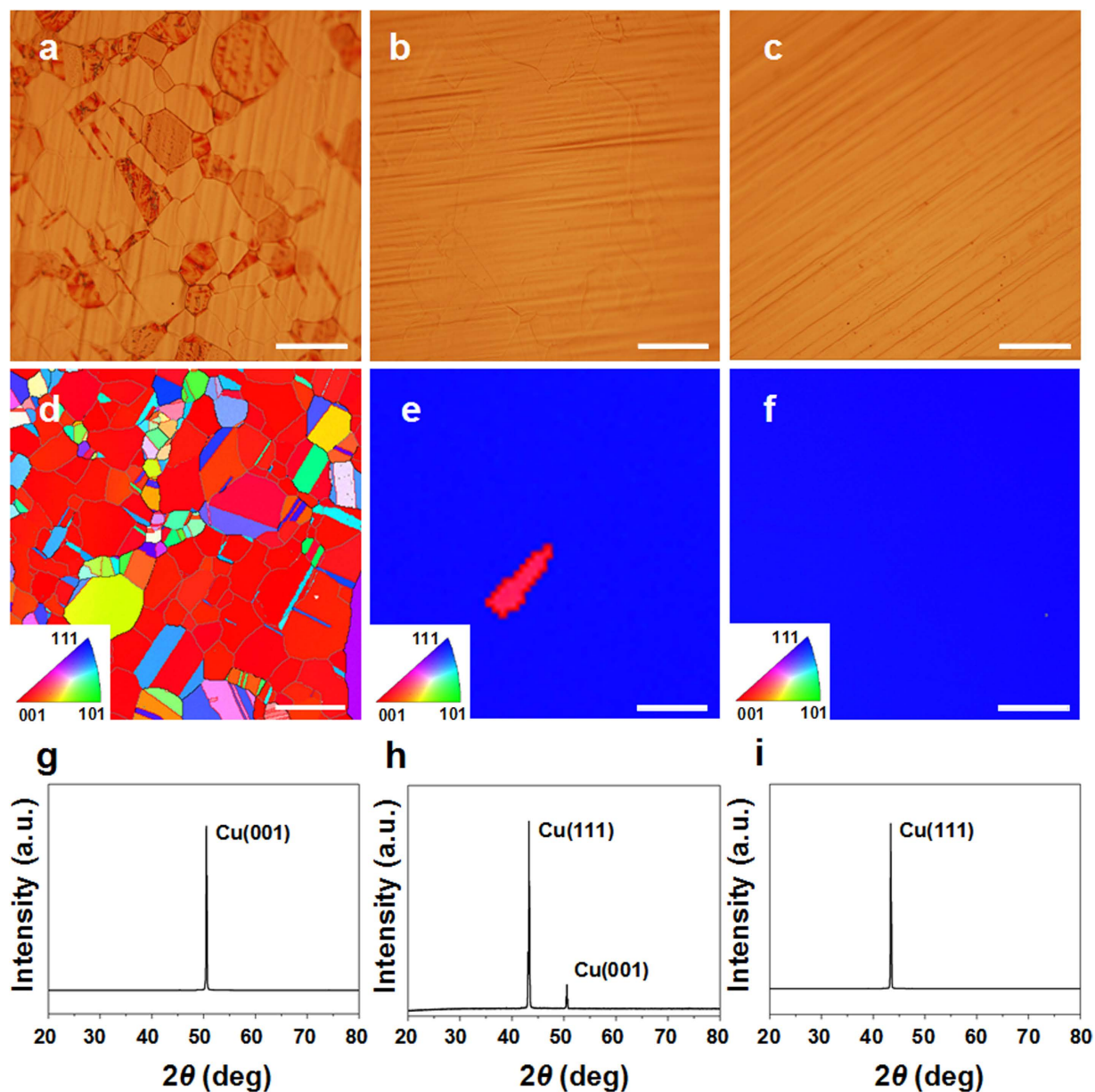
Figure 1. Surface morphology and structure characterizations of Cu foils annealed under 3 schemes.
Scheme 1: heating and annealing under Ar flow. Scheme 2: heating and annealing under H_2 and Ar flows,
respectively. Scheme 3: heating and annealing under H_2 flow. All the samples were heated up to 1040 °C under
ambient pressure within 40 min, then annealed at 1040 °C for 30 min. (**a–c**) Optical images of Cu foils annealed
under scheme 1–3. Scale bars, 50 μm. (**d–f**) EBSD orientation maps of Cu foils annealed under scheme 1–3. The
left inset in (**d–f**) shows the corresponding inverse pole figure for each map displayed. Grains marked blue are
oriented along plane Cu(111) while grains in red are along Cu(001). Scale bars, 200 μm (**d,e**); 500 μm (**f**). (**g–i**)
XRD profiles of Cu foils annealed under scheme 1–3. The measurements of EBSD and XRD were made from the
same area of Cu foils.

$$n_{do} = \left(\frac{1}{La}\right)^2 \tag{1}$$

$$L_a = [2.4 \times 10^{-10} nm^{-3}]\lambda_L^4 \left(\frac{I_D}{I_G}\right)^{-1} \tag{2}$$

where L_α is the grain size and λ_L is the excitation laser wavelength (532.15 nm). According to the I_D/I_G ratio (0.02),
the grain size L_α is calculated to be 963 nm while the defect density n_{do} is calculated as 1.08×10^8 cm^{-2}, which
shows a high-quality graphene[34] (Supplementary Fig. S6). To further evaluate the electrical quality of graphene
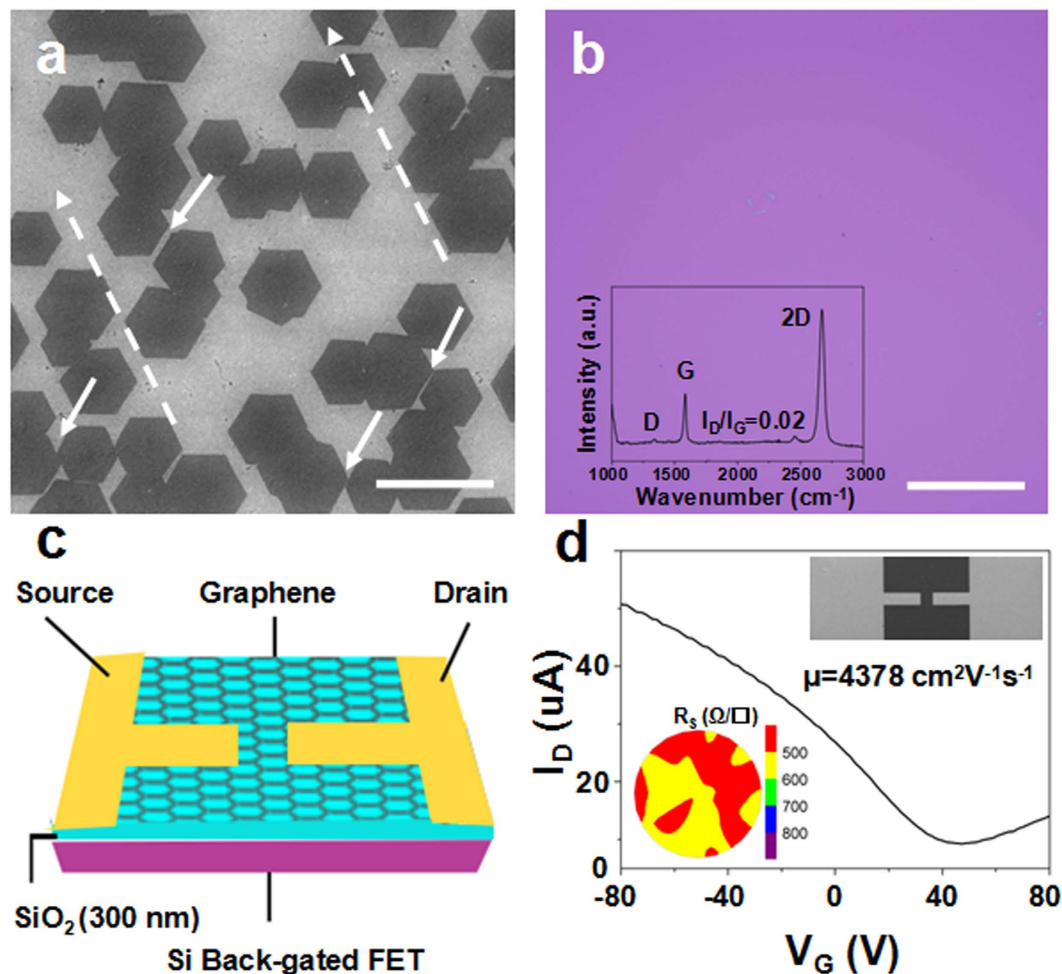
Figure 2. Optical and electrical characterizations of graphene grown on singe-domain Cu(111) substrate.
(**a**) Scanning electron microscope (SEM) image of a partial-coverage aligned graphene seeds on SiO$_2$/Si, where the white dashed lines indicate the orientations of graphene and the arrows point out the coalescence of adjacent islands. Scale bar, 20 μm. (**b**) Optical image of continuous graphene. The inset shows a representative single-point Raman spectrum. The negligible D band indicates the growth of high-quality graphene film. Scale bar, 20 μm. (**c**) Schematic of two-point back-gated field-effect-transistor (FET) device. (**d**) Current − voltage ($I_D − V_G$) curve for the continuous graphene grown on Cu(111)-FET measured at room temperature. The right inset shows the SEM image of the device and the left inset shows a representative sheet resistance distribution of graphene film transferred onto SiO$_2$/Si (1.5 mm in diameter).

films grown on Cu(111), we fabricated back-gated field-effect transistors (FETs) on a highly doped p-type silicon substrate with 300 nm oxide. The schematic of two-probe FET with length and width channels each of 50 μm is shown in Fig. 2c. Figure 2d shows the transfer characteristic of source-drain current (I_{ds}) versus gate voltage (V_{bg}) at room temperature and the right inset gives the SEM image of fabricated FET device. The carrier mobility of graphene grown on Cu(111) obtained from the Drude formula (see method) is 4378 cm^2 V^{-1} s^{-1}, comparable with the mobility of single-crystal graphene[35]. The corresponding Dirac point is 42 V, which indicates a p-type behavior of graphene film[36]. In order to evaluate the electrical property of graphene in a wide area inspection, the sheet resistance map (50 points in an area of 15 × 15 mm^2) of graphene film was measured by four-point probe measurement system (see method), as shown in the left inset of Fig. 2d. The sheet resistance of graphene grown on Cu(111) is around 500 Ω/□, showing an excellent electrical property[37,38].

For comparative study, we also investigated graphene growth on polycrystalline Cu(001) surface (Supplementary Fig. S7). The monolayer graphene was also produced on Cu(001). However, the seed shapes are randomly formed, without the domain orientation preference[8] (Fig. S7a). Even though there is no obvious contrast between the optical images of graphene grown on Cu(001) (Fig. S7b) and graphene grown on Cu(111) (Fig. 2b), the D-band of Raman spectra and the corresponding electrical properties show considerable difference. The I_D/I_G ratio of graphene on Cu(001) is as large as 0.38 (Fig. S7b), with the defect density n_{do} as high as 8.53 × 10^{10} cm^{-2}. Moreover, the carrier mobility is 870 cm^2 V^{-1} s^{-1} and the sheet resistance is 1000 Ω/□ (Fig. S7d). Therefore, the graphene electrical property grown on single domain Cu(111) is obviously superior to that grown on polycrystalline Cu(001)(Fig. S8). The electrical difference of the graphene films grown on Cu(111) and Cu(001) substrates would show different potential applications in electronic devices. For the graphene film grown
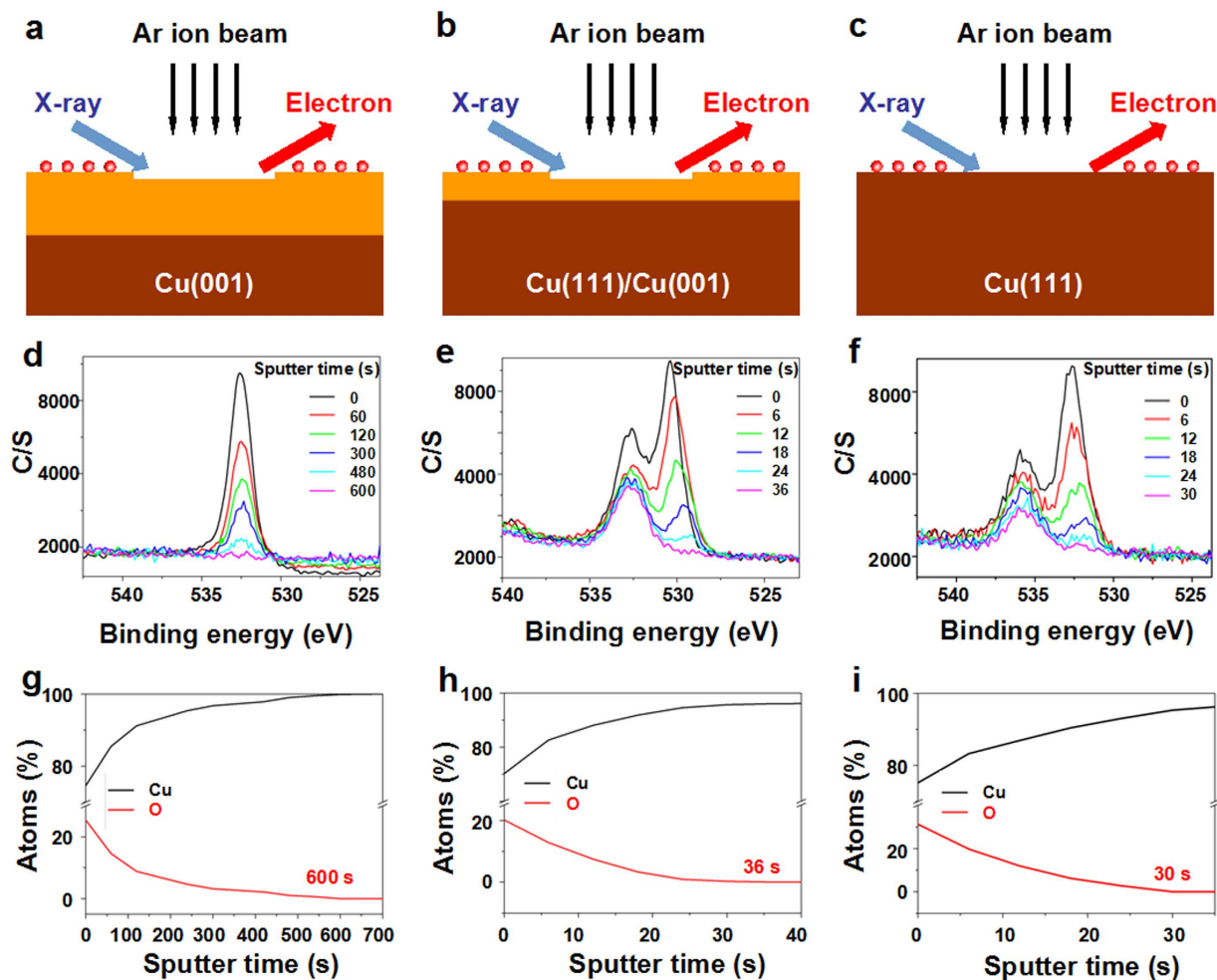
Figure 3. XPS analysis of the Cu foils annealed under 3 schemes. (**a–c**) Schematic structures for the XPS depth-profiling of three different thicknesses of copper oxides on corresponding substrate orientations. The orange layer refers to the copper oxides formed during annealing while the top red layer indicates the adsorption of oxygen from air. The thickness is not to scale. (**d–f**) Evolution of the O1s peaks as a function of sputter time. The Cu_2O peak is at 530.05 eV while the peak of 532.80 eV is attributed to H_2O[41–43]. (**g–i**) Relative atomic contents of O and Cu as a function of sputter time. Using SiO_2 as a reference, the corresponding thicknesses of oxidation layers for scheme 1–3 are measured to be 60 nm, 3.6 nm and 3 nm, respectively.

on Cu(111), the excellent electrical quality of graphene film can be used for flexible transparent electrodes[2,3]. While the graphene film on Cu(001) has larger sheet resistance, such graphene can be used to fabricate strain sensors, as graphene with low conductivity delivers higher sensing performance[39,40].

Discussion

To reveal the role of H_2 in the evolution of single domain Cu(111), the XPS depth-profiling examinations were taken on the Cu samples to measure the thickness of oxide layer along the vertical direction, as illustrated in Fig. 3. Due to the roughness of Cu surface, we use SiO_2 as a reference instead. The Ar-ion etching rate is about 6 nm min^{-1} based on the calibration of SiO_2. In scheme 1, the heating and annealing were introduced with Ar flow. Figure 3a shows the schematic structure of a thick oxide layer on Cu(001) substrate. As shown in Fig. 3d, the O1s peaks tend to decrease to zero with increasing the sputter time, indicating that the oxide layer is gradually removed by etching. The thickness of oxide layer on Cu(001) is calculated to be around 60 nm (Fig. 3g). After introducing H_2 during the heating process in scheme 2, the substrate obtains orientations of Cu(111) and Cu(001) ((Fig. 3b). Two O1s peaks were observed. The peak at B.E. (Binding energy) of 530.05 eV corresponds to Cu_2O bond[41], which shrinks quickly by Ar ion etching (Fig. 3e). The smaller peaks at higher B.E. of 532.80 eV correspond to H_2O bond due to the introduction of H_2[42,43]. According to the disappearance of O1s peak attributed to Cu_2O bond, the thicknesses of oxide layer in scheme 2 is estimated to be 3.6 nm (Fig. 3h), much thinner than that on the Cu(001) substrate as shown in Fig. 3g. Furthermore, when the heating and annealing were performed under H_2 flow in scheme 3, the substrate evolves into the single domain Cu(111) orientation (Fig. 3c). Similar with the case in Fig. 3e, the O1s peaks correspond to Cu_2O bond also decrease sharply by Ar ion etching (Fig. 3f) and the thicknesses of oxide layer on Cu(111) substrate remains nearly 3 nm. In addition, the decreasing oxygen contents from 0.52% (Scheme 1) to 0.44% (Scheme 3) was also observed by the energy dispersive spectroscopy

(EDS) (Fig. S9). Combination with the XPS depth-profiling and EDS results, it is believed that the Cu_2O layer plays a critical role in the orientation transition. With the thickness reduction of Cu_2O by introducing H_2, the substrate orientation changes from Cu(001) to Cu(111).

Since the extremely thin Cu_2O layers were both observed on the mix orientations of Cu(111)/Cu(001) (3.6 nm, scheme 2) and Cu(111) substrate (3 nm, scheme 3), maybe it originates from the air oxidation after the annealed Cu foils were extracted from the CVD chamber. By performing the same XPS depth-profiling examinations, the native oxide layer on the as-received Cu foil is estimated to be 6 nm[44] (see Fig. S10a,c in Supporting Information), indicating the oxide layers in scheme 2 and scheme 3 derive from the air oxidation[41]. Moreover, in order to prevent the air oxidation, a layer of graphene was deposited on the Cu foil before it was exposed to air in scheme 3, the absence of Cu_2O peaks in the XPS depth-profiling of as-grown graphene on Cu(111) surface implies that the graphene can play a role in protecting the underlying Cu from oxidation[45], further demonstrating that the introduction of H_2 (scheme 3) can completely remove the oxide layer on Cu surface (also see Fig. S10b,d in Supporting Information). It is noted that graphene can protect the surface of Cu substrate from oxidation in a short term due to its impermeability and thermal/chemical stability[45,46]. However, the Cu oxidation can still occur[47,48] because the carbon-metal interaction can accelerate electrochemical oxidation of Cu substrate through galvanic corrosion[46,49].

Based on the analysis of XPS depth-profiling, the orientation transition from Cu(001) to Cu(111) in Fig. 1 can be attributed to the thickness reduction of Cu_2O layer on Cu surface. When the Cu foil is exposed to abundant oxygen, the severe oxidation leads to the smaller grain size of only 5–10 μm. By decreasing the Cu_2O layer to around 60 nm, the grain size grows up to 50–100 μm. Meanwhile, this kind of Cu_2O layer tends to stabilize Cu(001) orientation[13], even annealed at 1040 °C for 180 min (Fig. S3a). Previous work revealed that oxidizing the Cu surface can induce the grain boundary pinning, freezing of the reconstruction of the Cu foil. Subsequent reduction of Cu foil under H_2, the delayed reconstruction can suddenly be unlocked[23]. As shown in Fig. 1e, once introducing H_2 to remove the oxide layer in scheme 2, the Cu(111) evolution is driven by the anisotropic force[50] and there is a grain boundary motion between Cu(111) and Cu(001) planes. After the Cu_2O layer is completely removed, the Cu substrate changes into the grain boundary-free Cu(111) single domain, as shown in Fig. 1f and Fig. S2. Moreover, once the Cu_2O layer is removed by H_2, our results show that the Cu(001) orientation can be transformed into Cu (111) in 1 min, as shown in Fig. S3.

The introduction of H_2 not only reduces the thickness of Cu_2O layer, but also reduces the density of nanopar-ticals generated during the heat treatment and makes Cu surface smooth (Figs S11 and S12), which is consistent with previous reports[15,51]. Preheated in Ar only, the Cu surface is rough and is decorated with a high density of nanoparticles. With the introduction of H_2, the density of nanoparticles is gradually decreasing from scheme 1 to scheme 3, and the roughness of Cu surface is improved obviously. Previous work indicated that the nanoparticles generated during heat treatment can affect the preferential attachment of graphene seeds (Fig. 2a and Fig. S5), where the ordered Cu(111) substrate can control the alignment of graphene islands by strong chemical bonds formed between the graphene edge and atomic step[15,52–54].

The graphene electrical property grown on polycrystalline Cu(001) is obviously inferior to that grown on single domain Cu(111), which can be attributed to three reasons. Firstly, the hexagonal lattice symmetry of Cu(111) surface matches well the honeycomb lattice of graphene (lattice mismatch of ~4%), enabling epitaxial graphene growth on single domain Cu(111)[10,23,55]. Secondly, carbon precipitation from the boundaries of Cu(001) grain leads to small elongated islands[56], as shown in Fig. S7b, degrading the uniformity of graphene. Thirdly, the graphene film on Cu(001) is grown by a lower temperature, leading to the increase of nucleation sites[57,58], as shown in Fig. S7a. The graphene grown on Cu(001) was grown at a relatively low temperature of 900 °C in this work. This is because that the increase of temperature leads to the disappearing of Cu(001) surface as shown in Fig. S3a. At such a low temperature, the graphitization is not as good as at higher temperatures.

The above analysis clearly shows that the oxygen on Cu surface tends to stabilize the Cu(001) orientation while impedes the evolution of single-domain Cu(111). To further understand the role of O_2 in crystal orientation control of Cu foils, we conducted the DFT calculations to study the effect of oxygen on the stabilities of Cu(001) and Cu(111), as shown in Fig. 4. Figure 4a illustrates the side and top view of the path for transition from Cu(001) to Cu(111). It can be seen that the marked angles of two structures are changing from 90° to 60°, while a transitional state (the corresponding angle is 65°) is located at the peak of energy barrier. Without considering the oxygen adsorbed on Cu, the surface energy of Cu(111) is 0.15 eV lower than Cu(001), indicating Cu(111) is more stable than Cu(001)[59]. This is the reason why the Cu(111) orientation can be formed once the oxygen is removed by H_2 flow, as shown in Fig. 1f,i and Fig. S3c–f. Moreover, the energy barrier between Cu(001) and Cu(111) is as high as 0.24 eV, which means a higher annealing temperature is necessary to overcome the barrier[11,12], indicated by Fig. S4a. However, once the attachment of oxygen on Cu surface is considered, the DFT calculation shows that the O/Cu(001) structure becomes 0.16 eV lower than O/Cu(111) structure, indicating O/Cu(001) is more stable than O/Cu(111). Moreover, the energy barrier (0.07 eV) increased by oxygen further impedes the orientation transition from Cu(001) to Cu(111). Our calculation explains the reason why the Cu substrate tends to form Cu(001) orientation once attached to the oxygen atoms, as shown in Fig. 1d,g and Fig. S3a,b.

Understanding the roles of O_2 and H_2 in monocrystallization of Cu substrate can be conductive to the achievement of large area Cu(001) or Cu(111) single-crystal, providing an ordered substrate for crystal orientation-controlled synthesis of well-aligned graphene seeds. For example, the introduction of oxygen on Cu surface induced the inch-sized Cu(001) single crystal[13] while the 12 cm Cu(111) surface was achieved with assistance of hydrogen[11], which enables the growth of square or hexagonal single-crystal graphene arrays. Considering that the grain boundaries can be suppressed by seamless coalescence of two identical orientations of islands, as demonstrated on the single-crystal Cu(111)[12], the synthesis of centimeter-size, even meter-size of single-crystalline graphene can be realized.
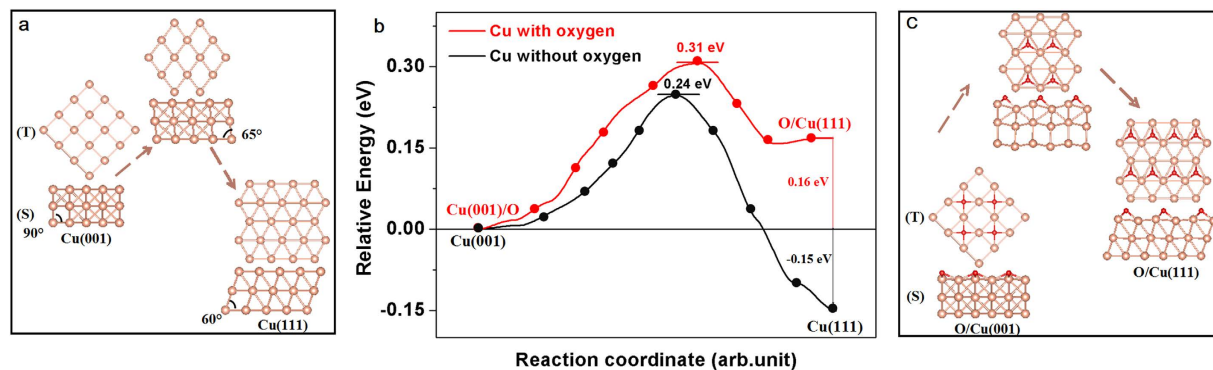
Figure 4. DFT calculations of the effect of oxygen on the orientation transition from Cu(001) to Cu(111).
The side (S) and top (T) views of the Cu surface without oxygen (**a**) and the favorable oxygen adsorption on
Cu surface (**c**). Note that the oxygen atoms become far away from Cu(111), indicating the weakly bond to the
Cu(111) surface. (**b**) The energy barrier between Cu(001) and Cu(111) without and with oxygen are 0.24 eV and
0.31 eV, respectively.

In summary, we have experimentally and theoretically demonstrated that the oxygen on Cu surface tends
to stabilize the Cu(001) orientation while impedes the evolution of Cu(111) single domain. The orientation
transition from Cu(001) to Cu(111) is attributed to the thickness reduction of Cu_2O layer on Cu surface. XPS
depth-profiling was performed to measure the thickness of Cu_2O layer while DFT calculations further reveal
that the O/Cu(001) is more stable than O/Cu(111). By removing the Cu_2O layer on Cu surface, the grain
boundary-free Cu(111) single domain can be obtained. The crystal orientation-controlled synthesis of hexagonal
graphene arrays has been further realized on the long-range ordered Cu(111). This work provides with a valuable
insight into the orientation transition of Cu substrates for growing high-quality graphene films.

Methods

Thermal treatments of Cu foils. The as-received commercially available 25 μm thick Cu foils (Kunshan
Luzhifa Electron Technology Co., Ltd. China) with a purity of 99.98% were loaded into a home-built CVD system
for thermal treatments. Before heating, the purging process was conducted in CVD chamber: Firstly the furnace
was evacuated to 0.1 Pa by a vacuum pump, then back filled with high pure Ar until ambient pressure, followed by
evacuating to 0.1 Pa again and filling with Ar. This purging process was repeated 3 times to minimize the trapped
air in CVD chamber. The detail of 3 schemes: Scheme 1, the sample was heated up to 1040 °C with the flow of 300
sccm of pure Ar then annealed at 1040 °C under the same Ar atmosphere for 30 min; Scheme 2, the sample was
heated up to 1040 °C with the flow of 300 sccm of pure H_2. After reaching 1040 °C, the H_2 was turned off and the
Cu foil was annealed under 300 sccm of pure Ar for 30 min; Scheme 3, the sample was heated up to 1040 °C with
300 sccm of pure H_2 then annealed at 1040 °C under the same H_2 atmosphere for 30 min. The gas atmosphere,
temperature, pressure, and cooling rate were carefully controlled by a CVD system.

Graphene growth and transfer. After thermal treatments of Cu foils, the furnace was maintained at
the same temperature (900 °C for graphene growth on Cu(001) and 1040 °C for graphene on Cu(111)). A small
amount of CH_4 (the concentration was diluted to 0.03–0.05% by H_2-Ar mixture gas) was introduced into the
CVD reactor at ambient pressure for 0.5–5 min. Finally the CVD furnace was cooled down to room temperature
at a rate of 0.3–0.9 °C/s after the heater power was shut down. After growth, graphene films grown on Cu(111)
and Cu(001) substrates were transferred to target substrates using the typical PMMA-mediated transfer-printing
technique. All the data was collected for samples with two desired growth temperatures 900 °C and 1040 °C.
Figure 2 data has been taken on graphene grown on Cu(111) at 1040 °C; Fig. S4 data has been taken on graphene
grown on Cu(001) at 900 °C.

Characterizations. X-ray diffractometer (German, D8 Advance) and SEM (CamScan, Apollo 300) equipped
with EBSD (HKLNordlysNano, Oxford) were used to analyze the macrotexture of Cu substrate. X-ray photoelec-
tron spectroscopy (XPS,ULVAC-PHI 5000 Versaprobe II) and EDS mapping (Quanta 250 FEG, USA) were used
to identify the surface elements of Cu substrates. The morphology of Cu surface was measured by Atomic Force
Microscope (Dimension 3100) at a scan rate of 1.2 Hz and 512 × 512 resolutions. The surface morphology of
the transferred graphene film was investigated through Scanning Electron Microscope (Quanta 400 FEG, USA)
and Optical Microscope (Olympus BX51, Japan). The optical transmittance of graphene/Cu(001) and graphene/
Cu(111) films with an area of 10 mm × 10 mm on glass was determined through UV-vis Spectroscopy (Perkin
Elmer Lambda 25, USA). Raman Spectrometer (LabRam HR800-UV-NIR, λ = 532.15 nm, France) was used to
identify the layer number and defect density of graphene/Cu(001) and graphene/Cu(111) films. The sheet resist-
ance maps (50 points in an area of 15 mm × 15 mm) of graphene films were obtained via Semi-automatic 4 probe
measurement system (CRESBOX, NAPSON) based on the van der Pauw method.

Device fabrication and transport measurements. The carrier mobilities of graphene grown on
Cu(001) and Cu(111) substrates were extracted from the back-gated field-effect-transistors (FETs) devices, with

channel length (L_C) 50 μm and channel width (L_W) 50 μm fabricated by standard photolithography technique. The electrical measurements of the devices were carried out at room temperature with the aid of Agilent B1500A semiconductor parameter analyzer. The gate voltage was applied through the doped Si substrate and the source-drain bias (V_{ds}) was constant at 0.01 V. The mobility was estimated by using the formula:

$$\mu_{FET} = \frac{L_{ch}}{w_{ch}\,C_G\,V_{DS}} \cdot g_m = \frac{L_{ch}}{w_{ch}\,C_G\,V_{DS}} \cdot \left.\frac{dI_D}{dV_{GS}}\right|_{V_{DS}=const} \tag{3}$$

where L_{ch} and W_{ch} are the channel length and channel width, respectively. C_G is the gate oxide capacitance per unit area, I_D is the source–drain current, V_{GS} is the gate voltage and V_{DS} is the source–drain voltage.

DFT calculations. To understand the transition mechanism, we search for the minimum energy pathway (MEP) between phases utilizing transition state theory as formulated in the generalized solid-state nudged elastic band (G-SSNEB) method implemented in the VTST extension of the Vienna ab initio simulation package (VASP). The calculations employed the projector augmented wave (PAW) method and the generalized gradient approximation (PBE-GGA) for electron exchange-correlation interaction. The energy cutoff for the plane wave functions is 460 eV with $7 \times 7 \times 1\,\Gamma$-centered Monkhorst-Pack grids, and a force acting on each atom of <0.001 eV/Å was used as the criterion of convergence in geometrical optimization. The Cu surface is modeled using a supercell approach, where we use a six-layered Cu slab with a vacuum region of 25 Å. Oxygen atoms are adsorbed on both sides of the slab, preserving inversion symmetry.

References

1. Li, X. *et al.* Large-area synthesis of high-quality and uniform graphene films on copper foils. *Science.* **324,** 1312–1314 (2009).
2. Bae, S. *et al.* Roll-to-roll production of 30-inch graphene films for transparent electrodes. *Nat. Nanotech.* **5,** 574–578 (2010).
3. Deng, B. *et al.* Roll-to-roll encapsulation of metal nanowires between graphene and plastic substrate for high-performance flexible transparent electrodes. *Nano Lett.* **15,** 4206–4213 (2015).
4. Huang, P. *et al.* Grains and grain boundaries in single-layer graphene atomic patchwork quilts. *Nature.* **469,** 389–392 (2011).
5. Kim, K. *et al.* Grain boundary mapping in polycrystalline graphene. *ACS Nano.* **5,** 2142–2146 (2011).
6. Yazyev, O. V. & Louie, S. G. Electronic transport in polycrystalline graphene. *Nat. Mater.* **9,** 806–809 (2010).
7. Yu, Q. *et al.* Control and characterization of individual grains and grain boundaries in graphene grown by chemical vapour deposition. *Nat. Mater.* **10,** 443–449 (2011).
8. Lee, J. H. *et al.* Wafer-scale growth of single-crystal monolayer graphene. *Science.* **344,** 286–289 (2014).
9. Iwasaki, T. *et al.* Long-range ordered single-crystal graphene on high-quality heteroepitaxial Ni thin films grown on MgO(111). *Nano Lett.* **11,** 79–84 (2011).
10. Ogawa, Y. *et al.* Domain structure and boundary in single-layer graphene grown on Cu(111) and Cu(100) Films. *J. Phy. Chem. Lett.* **3,** 219–226 (2012).
11. Brown, L. *et al.* Polycrystalline graphene with single crystalline electronic structure. *Nano Lett.* **14,** 5706–5711 (2014).
12. Nguyen, V. L. *et al.* Seamless stitching of graphene domains on polished copper (111) Foil. *Adv. Mater.* **27,** 1376–1382 (2015).
13. Wang, H. *et al.* Surface monocrystallization of copper foil for fast growth of large single-crystal graphene under free molecular flow. *Adv. Mater.* **28,** 8968–8974 (2016).
14. Hao, Y. *et al.* The role of surface oxygen in the growth of large single-crystal graphene on copper. *Science.* **342,** 720–723 (2013).
15. Gan, L. & Luo, Z. T. Turning off hydrogen to realize seeded growth of subcentimeter single-crystal graphene grains on copper. *ACS Nano.* **7,** 9480–9488 (2013).
16. Zhou, H. *et al.* Chemical vapour deposition growth of large single crystals of monolayer and bilayer graphene. *Nat. Commun.* **4,** 2096–3096 (2013).
17. Hao, Y. F. *et al.* Oxygen-activated growth and bandgap tunability of large single-crystal bilayer graphene. *Nat. Nanotech.* **11,** 426–431 (2016).
18. Xu, X. *et al.* Ultrafast growth of single-crystal graphene assisted by a continuous oxygen supply. *Nat. Nanotech.* **11,** 930–935 (2016).
19. Vlassiouk, I. *et al.* Role of hydrogen in chemical vapor deposition growth of large single-crystal graphene. *ACS Nano.* **5,** 6069–6076 (2011).
20. Gong, Y. *et al.* Layer-controlled and wafer-scale synthesis of uniform and high-quality graphene films on a polycrystalline nickel catalyst. *Adv. Funct. Mater.* **22,** 3153–3159 (2012).
21. Li, Q. *et al.* Growth of adlayer graphene on Cu studied by carbon isotope labeling. *Nano Lett.* **13,** 486–490 (2013).
22. Zhang, X. Y., Wang, L., Xin, J., Yakobson, B. I. & Ding, F. Role of hydrogen in graphene chemical vapor deposition growth on a copper surface. *J. Am. Chem. Soc.* **136,** 3040–3047 (2014).
23. Reckinger, N. *et al.* Oxidation-assisted graphene heteroepitaxy on copper foil. *Nanoscale.* **8,** 18751–18759 (2016).
24. Sharma, K. P. *et al.* Effect of copper foil annealing process on large graphene domain growth by solid source-based chemical vapor deposition. *J. Mater. Sci.* **51,** 7220–7228 (2016).
25. Maaβ, R. *et al.* Crystal rotation in Cu single crystal micropillars: *In situ* Laueand electron backscatter diffraction. *Appl. Phys. Lett.* **92,** 071905 (2008).
26. Li, X., Colombo, L. & Ruoff, R. S. Synthesis of graphene films on copper foils by chemical vapor deposition. *Adv. Mater.* **28,** 6247–6252 (2016).
27. Liu, Q. F., Gong, Y. P., Wilt, J. S., Sakidja, R. & Wu, J. Synchronous growth of AB-stacked bilayer graphene on Cu by simply controlling hydrogen pressure in CVD process. *Carbon.* **93,** 199–206 (2015).
28. Choi, D. S. *et al.* Effect of cooling condition on chemical vapor deposition synthesis of graphene on copper catalyst. *ACS. Appl. Mat. Interfaces.* **6,** 19574–19578 (2014).
29. Gao, L. *et al.* Efficient growth of high-quality graphene films on Cu foils by ambient pressure chemical vapor deposition. *Appl. Phys. Lett.* **97,** 183109 (2010).
30. Bhaviripudi, S., Jia, X. T., Dresselhaus, M. S. & Kong, J. Role of kinetic factors in chemical vapor deposition synthesis of uniform large area graphene using copper catalyst. *Nano Lett.* **10,** 4128–4133 (2010).
31. Ni, Z. *et al.* Graphene thickness determination using reflection and contrast spectroscopy. *Nano Lett.* **7,** 2758–2763 (2007).
32. Ferrari, A. C. *et al.* Raman spectrum of graphene and graphene layers. *Phys. Rev. Lett.* **97,** 187401 (2006).
33. Chen, J. *et al.* Defect scattering in graphene. *Phys. Rev. Lett.* **102,** 236805 (2009).
34. Hwang, J. Y., Kuo, C. C., Chen, L. C. & Chen, K. H. Correlating defect density with carrier mobility in large-scaled graphene films: Raman spectral signatures for the estimation of defect density. *Nanotechnology* **21,** 465705 (2010).
35. Li, X. *et al.* Large-area graphene single crystals grown by low-pressure chemical vapor deposition of methane on copper. *J. Am. Chem. Soc.* **133,** 2816–2819 (2011).

36. Suk, J. W. *et al.* Enhancement of the electrical properties of graphene grown by chemical vapor deposition via controlling the effects of polymer residue. *Nano Lett.* **13,** 1462–1467 (2013).
37. Li, X. *et al.* Transfer of large-area graphene films for high-performance transparent conductive electrodes. *Nano Lett.* **9,** 4359–4363 (2009).
38. Lee, Y. B. *et al.* Wafer-scale synthesis and transfer of graphene films. *Nano Lett.* **10,** 490–493 (2010).
39. Li, Q. *et al.* Wide range strain sensors based on highly transparent and supremely stretchable graphene/Ag-nanowires hybrid structures. *Small.* **12,** 5058–5065 (2016).
40. Chen, Z. *et al.* Three-dimensional flexible and conductive interconnected graphene networks grown by chemical vapor deposition. *Nat. Mater.* **10,** 424–428 (2011).
41. Chavez, K. L. & Hess, D. W. A novel method of etching copper oxide using acetic acid. *J. Electrochem. Soc.* **148,** G640–G643 (2001).
42. Andersson, K. *et al.* Bridging the pressure gap in water and hydroxyl chemistry on metal surfaces: The Cu(110) case. *J. Phys. Chem. C.* **111,** 14493–14499 (2007).
43. Ammon, C., Bayer. A., Steinrück, H. P. & Held, G. Low-temperature partial dissociation of water on Cu(1 1 0). *Chem. Phys. Lett.* **377,** 163–169 (2003).
44. Platzman, I., Brener, R., Haick, H. & Tannenbaum, R. Oxidation of polycrystalline copper thin films at ambient conditions. *J. Phys. Chem. C.* **112,** 1101–1108 (2008).
45. Chen, S. *et al.* Oxidation resistance of graphene-coated Cu and Cu/Ni alloy. *ACS Nano.* **5,** 1321–1327 (2011).
46. Schriver, M., Regan, W., Gannett, W. J., Zaniewski, A. M., Crommie, M. F. & Zettl. A. Graphene as a long-term metal oxidation barrier: Worse than nothing. *ACS Nano.* **7,** 5763–5768 (2013).
47. R. Ramírez-Jínenez. *et al.* Interference enhanced Raman effect in graphene bubbles. *Carbon.* **105,** 556–565 (2016).
48. Ogawa, S. *et al.* Graphene growth and carbon diffusion process during vacuum heating on Cu(111)/Al$_2$O$_3$ substrates. *Jpn. J. Appl. Phys.* **52,** 110122 (2013).
49. Sun, W. *et al.* Inhibiting the corrosion-promotion activity of graphene. *Chem. Mater.* **27,** 2367–2373 (2015).
50. Sonnweber-Ribic, P., Gruber, P., Dehm, G. & Arzt, E. Texture transition in Cu thin films: Electron backscatter diffraction vs. X-ray diffraction. *Acta. Mater.* **54,** 3863–3870 (2006).
51. Wang, H. *et al.* Controllable synthesis of submillimeter single-crystal monolayer graphene domains on copper foils by suppressing nucleation. *J. Am. Chem. Soc.* **134,** 3627–3630 (2012).
52. Dai, J. *et al.* How Graphene islands are unidirectionally aligned on the Ge(110) surface. *Nano Lett.* **16,** 3160–3165 (2016).
53. Zhang, X., Xu, Z. W., Hui, L., Xin, J. & Ding, F. How the orientation of graphene is determined during chemical vapor deposition growth. *J. Phys. Chem. Lett.* **3,** 2822–2827 (2012).
54. Murdock, A. T. *et al.* Controlling the orientation, edge geometry, and thickness of chemical vapor deposition graphene. *ACS Nano.* **7,** 1351–1359 (2013).
55. Wofford, J. M., Nie, S., McCarty, K. F., Bartelt, N. C. & Dubon, O. D. Graphene Islands on Cu foils: the interplay between shape, orientation, and defects. *Nano Lett.* **10,** 4890–4896 (2010).
56. Han, Z. *et al.* Homogeneous optical and electronic properties of graphene due to the suppression of multilayer patches during CVD on copper foils. *Adv. Funct. Mater.* **24,** 964–970 (2014).
57. Lavin-Lopez, M. P. *et al.* Synthesis and characterization of graphene: influence of synthesis variables. *Phys. Chem. Chem. Phys.* **16,** 2962–2970 (2014).
58. Hu, B. *et al.* Epitaxial growth of large-area single-layer graphene over Cu(111)/sapphire by atmospheric pressure CVD. *Carbon.* **50,** 57–65 (2012).
59. Vitos, L., Ruban, A. V., Skriver, H. L. & Kollár, J. The surface energy of metals. *Surface Science.* **411,** 186–202 (1998).

Acknowledgements

Author Contributions

J.H., J.X. and L.L. conceived and designed the experiments. J.H. and J.X. directed the experiments. J.H. carried out most of the experiments (including thermal treatments of Cu foils, CVD graphene growth, Raman mapping, optical microscopy imaging and SEM imaging, Ultraviolet–visible absorption, XRD, EBSD) and data analysis. J.H., J.X., Y.G. and F.L. contributed to device fabrication and electrical measurement. W.L. and Y.Z. carried out the X-ray photoelectron spectroscopy and L.S conducted the DFT calculations. J.H., J.X., Z.U., Q.L. and L.L. wrote the manuscript. All authors discussed the results and commented on the manuscript.

Additional Information

Supplementary information accompanies this paper at http://www.nature.com/srep

Competing Interests: The authors declare no competing financial interests.

How to cite this article: Hu, J. *et al.* Roles of oxygen and hydrogen in crystal orientation transition of copper foils for high-quality graphene growth. *Sci. Rep.* **7,** 45358; doi: 10.1038/srep45358 (2017).

Publisher's note: Springer Nature remains neutral with regard to jurisdictional claims in published maps and institutional affiliations.